ELSEVIER

Journal of Nuclear Materials 302 (2002) 9–19

journal of nuclear materials

www.elsevier.com/locate/jnucmat

Correlation between microstructure and corrosion behavior of Zr–Nb binary alloy

Yong Hwan Jeong [a,*], Kyoung Ok Lee [a], Hyun Gil Kim [b]

[a] *Zirconium Fuel Cladding Team, Korea Atomic Energy Research Institute, P.O. Box 105, Yusong, Daejeon 305600, South Korea*
[b] *Department of Material Science and Engineering, Yonsei University, Sinchon-dong 134, Seoul 120749, South Korea*

Received 19 April 2001; accepted 27 December 2001

Abstract

To investigate the correlation between microstructure and corrosion characteristics of Zr–Nb alloy, the microstructural observation and corrosion test with the change of cooling rate from beta temperature and the variation of Nb content were performed. The oxide characterization was also carried out by synchrotron XRD and TEM. When the Nb is contained less than solid solution limit (0.6 wt%) in Zr matrix, the difference of corrosion rate was not observed in spite of showing the significant changes of microstructures with cooling rate. While, when the Nb content in the alloy is more than 0.6 wt%, the corrosion properties were deteriorated with increasing the supersaturated Nb concentration in matrix and increasing the area fraction of β_{Zr}. Also it was observed that the supersaturated Nb in matrix was more effective to decrease the corrosion resistance than the β_{Zr} phase in the same Nb containing alloy, while the equilibrium Nb concentration below solubility limit in the matrix played an important role to enhance the corrosion resistance. During the corrosion testing in steam at 400 °C, the formation of β_{Nb} phase in water-quenched specimen would result in the reduction of Nb concentration in matrix. Thus, the corrosion resistance is enhanced with the formation of β_{Nb} phase. It is suggested from this study that the equilibrium Nb concentration below solubility limit in α matrix would be a more dominant factor in the enhancement of corrosion resistance than β phase (β_{Nb} or β_{Zr}), supersaturated Nb, precipitate, and internal microstructure such as twin, dislocation and plate.

PACS: 81.65.M; 81.65.K; 42.81.B

1. Introduction

Zirconium alloys have been widely used as nuclear fuel cladding tubes and structural materials due to low neutron absorption cross-section, superior corrosion resistance and high mechanical strength etc. Among them, Zircaloy-4 alloy has been used as nuclear fuel cladding materials for several decades without any significant problems in pressurized water reactor. However more advanced Zr-based alloys are recently required for the more severe operating condition such as higher burn-up, increased operation temperature, and high pH operation. As a substitute for Zircaloy-4, several new Zr alloys such as Zirlo (Zr–1.0Nb–1.0Sn–0.1Fe) [1], M5 (Zr–1Nb–O) [2] and NDA (Zr–0.1Nb–1.0Sn–0.27Fe–0.16Cr) [3] were developed and are being tested in reactor. Like this, most new Zr alloys that are being developed contain the Nb element. However, it is reported that the corrosion behavior of Nb-containing Zr alloy is very sensitive to the microstructures that could be changed by heat treatment.

Up to now, the correlation between microstructural changes and corrosion behaviors in Zr–Nb binary alloys, in particular Zr–2.5Nb alloy, have been investigated by many workers [4–11]. It is reported that the

* Corresponding author. Tel.: +82-42 868 2322; fax: +82-42 863 0565.
E-mail address: yhjeong@kaeri.re.kr (Y.H. Jeong).

0022-3115/02/$ - see front matter
PII: S0022-3115(02)00703-1

Table 1
Chemical composition of Zr–Nb alloys used in this study

Alloy	Nb (wt%)	O (ppm)	Fe (ppm)	N (ppm)	C (ppm)	Balance
0.5Nb	0.48	520	420	<25	36	Zr
1.0Nb	1.08	500	420	<25	38	Zr
2.0Nb	1.95	543	410	<25	39	Zr
3.0Nb	2.93	510	430	<25	35	Zr

martensitic structure where all the added Nb is supersaturated in the matrix and β_{Zr} (~20 wt% Nb) phase accelerate the oxidation of Zr alloy [4–6], while β_{Nb} phase decreases the oxidation of Zr alloy [7]. It is known that β_{Nb} phase is produced by aging of quenched Zr–Nb alloy having martensitic structure below monotectoid temperature (610 °C) [8,9], or by the decomposition of β_{Zr} phase to ($\alpha_{Zr} + \beta_{Nb}$) phases when β_{Zr} phase is annealed [10,11]. Also, Urbanic [4] reported that the corrosion resistance was enhanced with precipitation of β_{Nb} phase in Zr–2.5 wt% Nb pressure tube under irradiation condition. These studies are mainly focused on the Zr–2.5 wt% Nb alloy that is being used as a pressure tube material for CANDU-PHW reactors. However, the correlation between oxide characteristics and microstructure or microchemistry such as beta phase, Nb-containing precipitate, and Nb concentration in matrix is not well understood in Zr–Nb alloys.

Thus, for better understanding the correlation between microstructure and corrosion behavior, it is necessary to do the systematic study with the variation of Nb content and cooling rate in Zr–Nb binary alloys. Therefore, in this study, the specimens having different microstructure were prepared with the variation of cooling rate and Nb content. And the corrosion test, the microstructural study, and the oxide characterization for the specimens were performed to investigate the effect of the soluble Nb content, β phase, and precipitates on the corrosion resistance. In addition, the microstructural change such as the formation of β_{Nb} phase and the decomposition of β_{Zr} phase during corrosion test, and their effect on the corrosion were also investigated.

2. Experimental procedure

Table 1 shows the chemical composition of Zr alloys used in this study. High purity (99.99%) niobium was added to prepare the Zr–*x*Nb binary alloy containing 0.5, 1.0, 2.0 and 3.0 wt% Nb. Other elements such as O, Fe, N, and C were introduced from the sponge Zirconium. Small ingots of 300 g were rolled to ≈1.0 mm

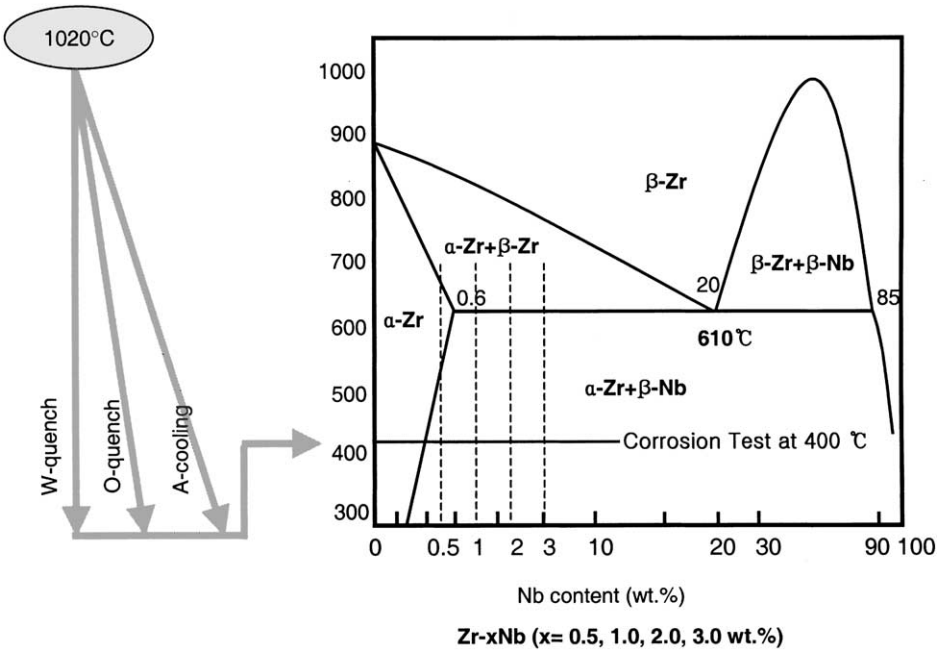

Fig. 1. Experimental procedure and phase diagram of Zr–Nb alloy system.

thickness sheets. These rolled sheet specimens were sealed in evacuated quartz capsules and then heat treated as shown in Fig. 1.

The specimens for autoclave corrosion testing were polished by SiC paper to remove surface contaminant and then corroded in a static autoclave under the condition of 400 °C steam and 1500 psi. The microstructural observation and the analysis for the precipitates were performed using the polarized optical microscopy and transmission electron microscopy. The observation of optical microstructure was performed for the perpendicular section to the rolling direction of specimens, and the specimens were etched with a solution containing 10 vol% HF, 45 vol% HNO_3 and 45 vol% H_2O. Thin foils for transmission electron microscopy of matrix were prepared by grinding up to 70 μm thickness and then electrolytically polished with a mixed solution of 90 vol% ethanol and 10 vol% perchloric acid using twin-jet electro-polisher at −40 °C. The analysis of chemical composition for the precipitate was performed using EDS in the TEM, and the area fraction of second phase was measured using the image analyzer from the TEM photographs.

To investigate the oxide characteristics, the oxide crystallography and the oxide microstructure on the corroded specimens having the same weight gain were analyzed by synchrotron XRD and TEM, respectively. The synchrotron X-ray scattering experiments were carried out at beamline 5C2 at Pohang Light Source in Korea for the corroded specimens having the equal weight gain of 10 mg/dm^2. For the TEM observation on the oxide, the sections forming oxide in the corroded samples having the weight gain of 20 mg/dm^2 were put together and sealed in the thickness of about 300 μm for the perpendicular direction to the oxide/metal interface. This specimen was mechanically polished in the thickness of 20–30 μm and then ion-milled.

3. Results and discussion

3.1. Microstructure characteristics with cooling rate and Nb content

Fig. 2 shows the optical microstructures of the specimens that were heat treated with different cooling rate

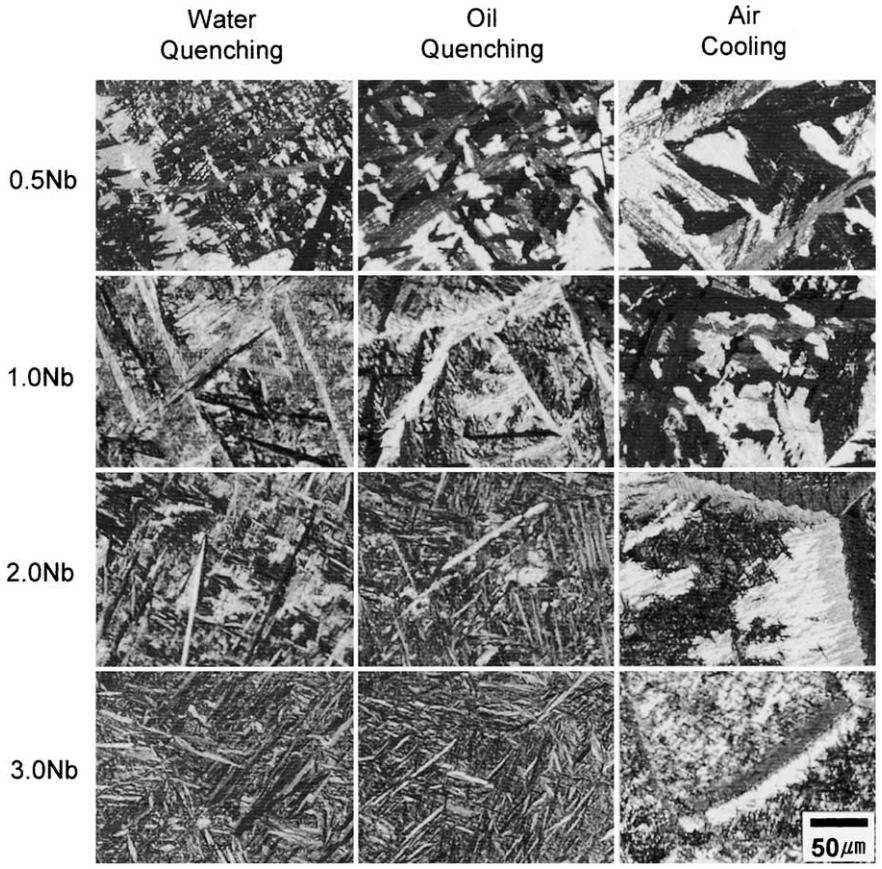

Fig. 2. Optical micrographs of Zr–xNb alloys with cooling rate.

from beta temperature (1020 °C) and different Nb content. In the case of water-quenched specimens, the martensitic structure was formed in all tested alloys. Oil-quenched specimens containing more than 1.0 wt% Nb also showed martensitic structures with coarser plate than those in water-quenched specimens in the same Nb content. In the Zr–0.5 wt% Nb alloys, Widmanstatten structure was formed in the oil-quenched specimen and the water-quenched specimen. In the same cooling rate, the length and width of plate get fine with increasing Nb content.

In the optical microstructures, it is not easy to describe the difference between martensitic structure and Widmanstatten structure. Therefore, to investigate the microstructure more clearly, TEM observation was performed for the Zr–xNb ($x = 1.0$, 3.0 wt% Nb) alloys, as shown in Fig. 3. For the water-quenched and the oil-quenched alloys having fast cooling rate, martensitic structure was formed in both alloys. However, there is a difference in the morphology with Nb content. For the shape change during martensitic transformation, the reverse stress was applied in the vicinity of the transformation field, and to relieve the stress, plastic deformation is generated. It is known that this plastic deformation can be occurred by the movement of dislocation, where the movement of perfect dislocation produces slip and the movement of partial dislocation generates stacking fault or internal twin [12]. Also it was reported that the M_s temperature decreased with increasing Nb content [13] and at the low temperature it is not easy to form all dislocation needed to slip deformation. Therefore, the plastic deformation of the increased Nb containing alloys at low temperature would be occurred by not slip system but twin system [14]. In this study, twin free martensite having high dislocation density was observed in Zr–1.0 wt% Nb alloys and twinned Martensite was formed in Zr–3.0 wt% Nb alloys as shown in Fig. 3. This result, as mentioned above, means that M_s temperature is getting low with increasing Nb content from 1.0 to 3.0 wt% as long as the alloy do not have enough dislocation to make a slip. And the air-cooled specimens that cooling rates were slow showed Widmanstatten structure in both 1.0 and 3.0 wt% Nb alloys.

For the chemical analysis, EDS analysis for the matrix and the second phase of Zr–xNb ($x = 1.0$, 3.0 wt%) was performed. It was reported by Choo [15] that the added Nb till 5 wt% was supersaturated in matrix without the formation of second phase or precipitate when the cooling rate was so fast. In this study the formation of the second phase or precipitate was not also observed in water-quenched specimens. Accordingly it is considered that all the added Nb is supersaturated in the matrix. However, in the air-cooled specimens (Fig. 3(c) and (f)) of both 1.0Nb and 3.0Nb alloys, white band shaped phase and black line shaped phase were ranged alternatively, and these phases were identified as α_{Zr} and β_{Zr} phase respectively from the re-

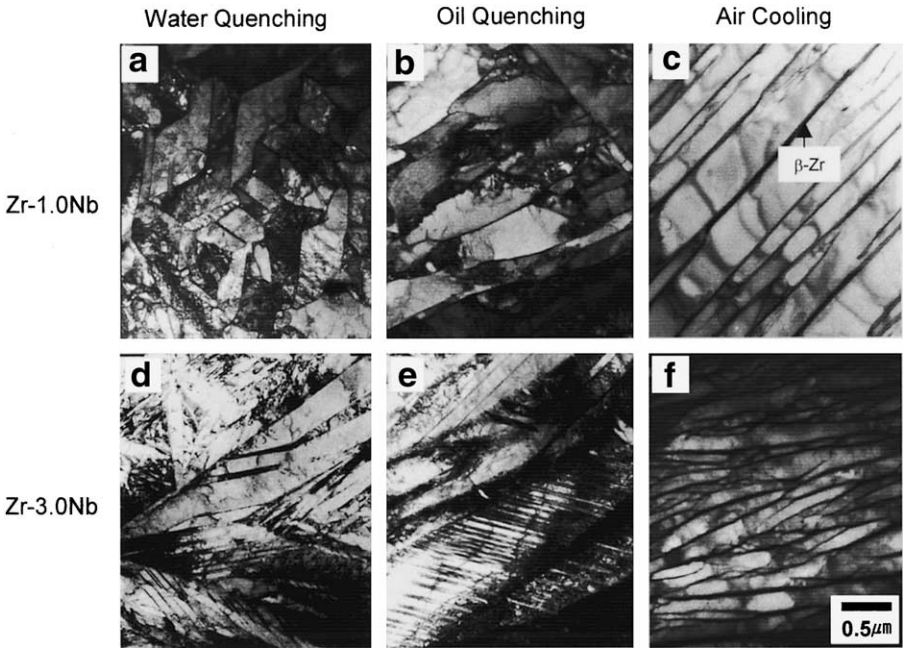

Fig. 3. TEM micrographs of Zr–xNb alloy with cooling rate.

Table 2
Area fraction of β_{Zr} phase in air-cooled Zr–xNb ($x = 1.0$, 3.0 wt%) alloys

Zr–1.0 wt% Nb	Zr–3.0 wt% Nb
8.6%	23.8%

sults of EDS analysis. The area fraction of the second phase calculated by the image analyzer was 8.6 and 23.8 vol% in Zr–1.0 wt% Nb alloy and Zr–3.0 wt% Nb alloy respectively, as shown in Table 2.

To analyze the supersaturated Nb concentration in matrix, EDS analysis was performed for the water-quenched, oil-quenched, and air-cooled specimens. It was not successful to analyze the exact Nb concentration in matrix owing to the limited resolution of EDS and scattering of results. However, as shown in Fig. 4, it can be expected that in the specimens having Nb content more than 0.6 wt%, the supersaturated Nb concentration in matrix would be decreased with decreasing the cooling rate, and the Nb concentration within α_{Zr} in the air-cooled specimen, which was transformed by diffusional transformation, would reach to about the equilibrium concentration of Nb. When Nb content is less than solubility limit, all the added Nb would exist as equilibrium state without the supersaturated Nb in even the water-quenched specimen regardless of cooling rate. In Fig. 4, the relative value is based on the Nb concentration of air-cooled specimen that represent the equilibrium Nb concentration below solubility limit.

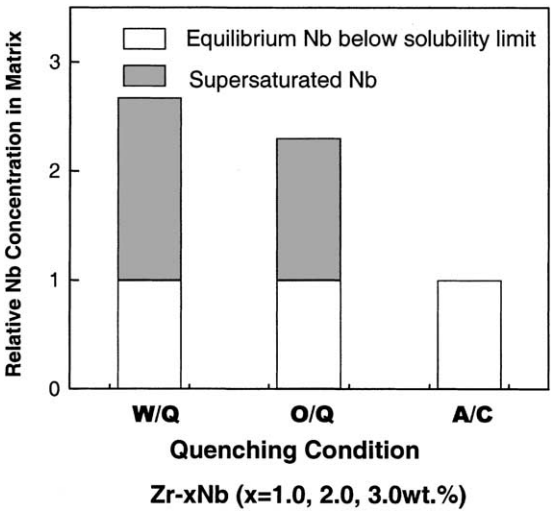

Fig. 4. Relative Nb concentration in α matrix of Zr–xNb ($x = 1.0$, 2.0, 3.0 wt%) alloys with various cooling rate. Relative value is based on the Nb concentration of air-cooled specimen that represent the equilibrium Nb concentration below solubility limit.

3.2. Corrosion behaviors with cooling rate and Nb content

To investigate the effect of microstructural change on corrosion behavior of the alloy with variation of cooling rates and Nb contents, the corrosion test was performed for the Zr–xNb ($x = 0.5$, 1.0, 2.0, 3.0 wt%) alloys heat-treated as shown in Fig. 1. Fig. 5 shows the corrosion behavior of four kinds of Zr–xNb ($x = 0.5$, 1.0, 2.0, 3.0 wt%) alloys in steam at 400 °C for 60 days. Generally, the transition of corrosion rate occurs in Zircaloy system alloys when weight gain come to be about 30–40 mg/dm^2 [16]. But the transition of corrosion rate in these alloys was not seen until the weight gain was more than 150 mg/dm^2. This is coincident with the reported result [17] that a sudden acceleration of corrosion rate (transition) was not observed in Zr–Nb alloy system.

The effects of cooling rate on corrosion behaviors of the specimens (Fig. 5(b)–(d)) having the Nb more than 1.0 wt% were different from that of the specimen (Fig. 5(a)) having Nb content of 0.5 wt%. In the corrosion test of Zr–0.5 wt% Nb alloy system, the weight gains showed a similar value regardless of cooling rate. It was considered that all the added Nb was distributed uniformly in matrix in all cooling condition because the added Nb was less than solid solution limit (0.6 wt%). In the case of Zr–Nb alloy system containing Nb more than 0.6 wt%, it was observed that the weight gain of water-quenched specimen was similar to the value of the oil-quenched specimen but much higher than that of the air-cooled specimen. As mentioned above, the formation of the second phase particle or precipitate was not observed in the specimens of which the cooling rates were as fast as those in water quenching and oil quenching, so it is thought that the added Nb more than 0.6 wt% was supersaturated in the matrix. And in the air-cooled specimens, the film-shaped β_{Zr} phase containing about 20 wt% Nb was precipitated and the Nb concentration in the matrix was lowered to the equilibrium concentration due to slow cooling rate as shown in Fig. 3. Accordingly it was considered that Nb concentration in the α matrix of air-cooled specimens was lower than those of the water-quenched specimen and oil-quenched specimen. It is known that the corrosion resistance is greatly affected by the Nb concentration in the α matrix; concretely speaking the corrosion is accelerated with increasing the supersaturated Nb concentration in matrix [6]. Consequently, it is considered that the corrosion resistances of water-quenched and oil-quenched specimens of which cooling rates are so fast are lower than that of the air-cooled specimens of which cooling rate are slower relatively.

It was observed that the weight gain increased with increasing Nb content in all the cooling conditions. Fig. 6 shows the expected amount of supersaturated Nb in the matrix with variation of Nb content in the water-quenched specimen (Fig. 6(a)) and the relative fraction

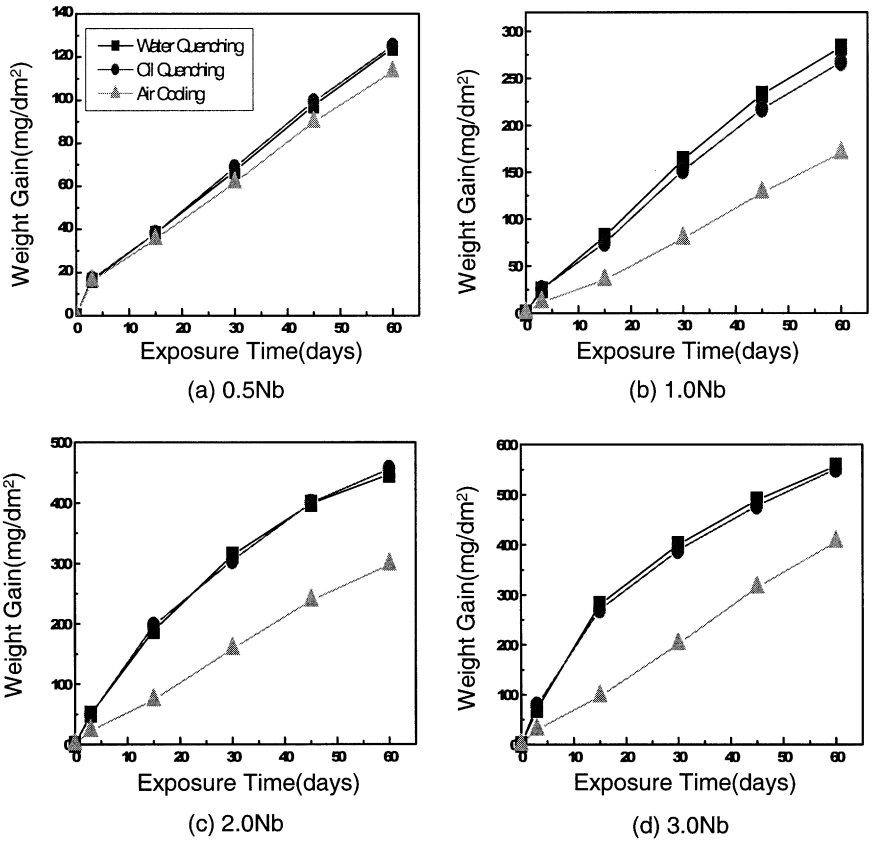

Fig. 5. The effect of cooling rate on the corrosion behavior of Zr–*x*Nb alloys corroded at 400 °C steam for 60 days.

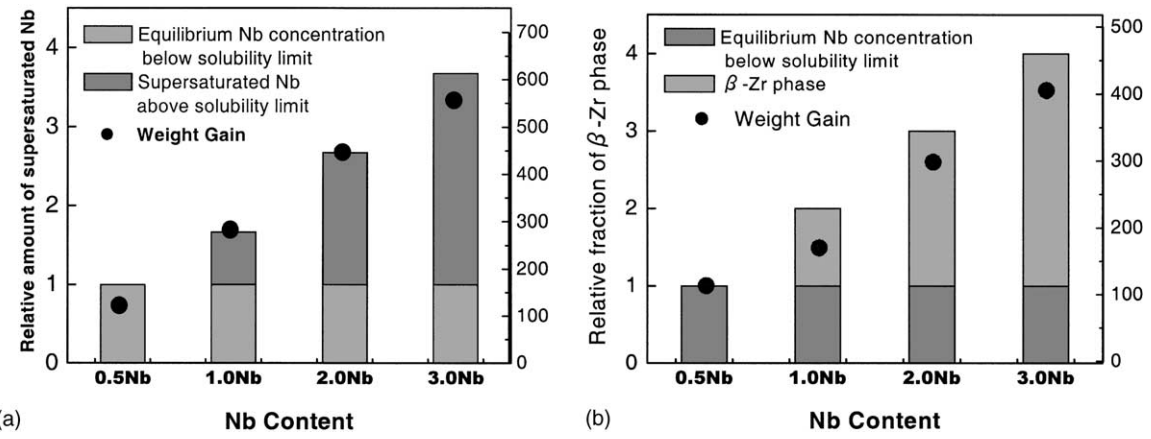

Fig. 6. (a) Expected amount of supersaturated Nb in matrix with variation of Nb content in water-quenched and (b) relative fraction of β_{Zr} in air-cooled specimens. Relative value is based on the that of 0.5Nb alloy.

of β_{Zr} phases in the air-cooled specimen (Fig. 6(b)). In Fig. 6, the relative value is based on the that of 0.5Nb alloy. As mentioned above, in the water-quenched and oil-quenched specimens the supersaturated Nb concentrations in matrix would be increased with increasing Nb contents. Therefore, the weight gain increased with increasing Nb content in the same cooling condition. However, in the air-cooled specimen the Nb concen-

tration in the α matrix would be almost identical in spite of increasing Nb content, and β_{Zr} phases were precipitated in the both alloys of 1.0 and 3.0 wt% Nb. It was observed that the amount of β_{Zr} phase produced per unit area increased about three times as much as Nb content increased from 1.0 to 3.0 wt%. This results coincided with the report that the more the amount of β_{Zr} phase increased the less corrosion resistance was [4]. Even though the air-cooled specimens containing 1.0 and 3.0 wt% Nb would have the same equilibrium Nb concentration in the α matrix, the weight gain of air-cooled 3.0 wt% Nb alloy was higher than that of air-cooled 1.0 wt% Nb alloy owing to high amount of β_{Zr} phase.

3.3. Oxide characterization by synchrotron XRD and TEM

Pilling–Bedworth (PBW) ratio means volume ratio of metallic oxide versus metal, and PBW ratio of ZrO_2/Zr is as greatly high as 1.56. So the high compressive stress due to volume expansion accompanied by formation of oxide is applied to the oxide formed in the early corrosion. In the early stage of corrosion, the plenty of tetra-ZrO_2 that is meta-stable phase and has protective property is formed. However, as the oxidation is getting progressed, the protective tetra-ZrO_2 is transformed to mono-ZrO_2 having non-protective property. It is known that the corrosion is accelerated by this change of oxide structure [18].

Fig. 7 shows the crystallography of oxide measured by synchrotron X-ray scattering for the water-quenched and air-cooled Zr–1.0 Nb alloy having the weight gain of about 10 mg/dm^2 respectively. The (1 1 1) tetra-ZrO_2 peak was observed in the vicinity of 27° as shown in Fig. 7. The volume fraction of protective tetra-ZrO_2 measured was higher in the air-cooled specimen (14.9%) than in the water-quenched specimen (5.1%). This trend matched up to the result that the corrosion resistance of the air-cooled specimen was better than that of water-quenched specimen. Even though they have an equal oxide thickness, the intensity of (1 1 1) mono-ZrO_2 in the water-quenched specimen that showed the fast corrosion rate was much higher than that in the air-cooled specimen. Therefore, it is considered that the preferential

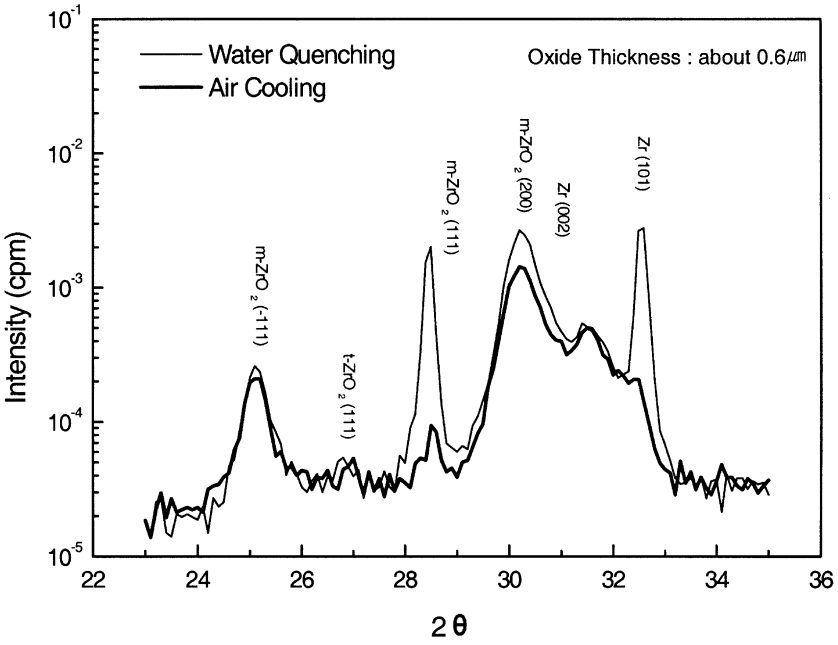

	Water Quenching	Air Cooling
Ratio of (tetra/mono) ZrO_2	5.1 %	14.9 %

Fig. 7. Syncrotron X-Ray diffraction pattern with cooling rate in Zr–1.0 wt% Nb alloys corroded at 400 °C steam (weight gain: about 10 mg/dm^2).

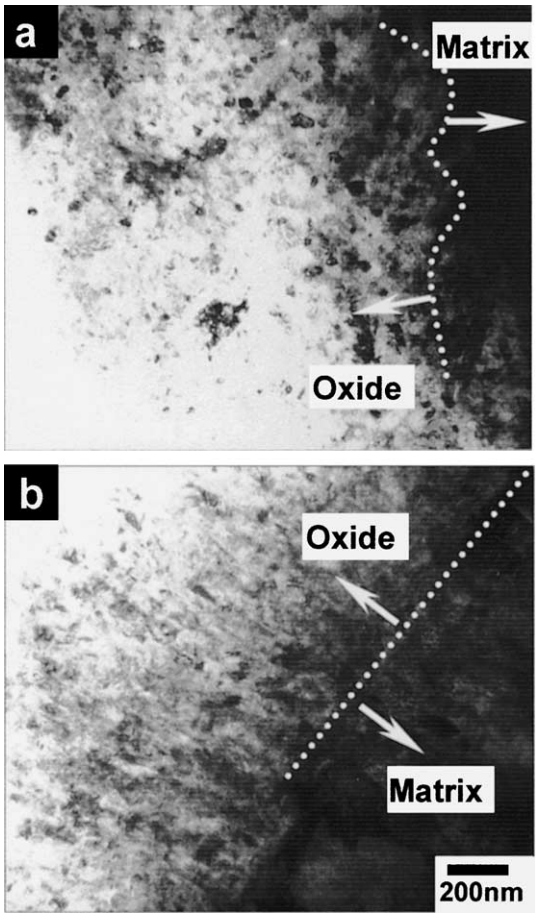

Fig. 8. Cross-sectional TEM micrographs of Zr–1.0 wt% Nb alloy oxide grown in steam at 400 °C (weight gain: 20 mg/dm^2): (a) water-quenched specimen (b) air-cooled specimen.

growth of (1 1 1) mono-ZrO_2 has a close relationship with the fast corrosion rate in the water-quenched specimen.

Many workers have investigated the oxide characteristics by using TEM and SEM to understand corrosion mechanisms. [19–21]. In this study, the observation on oxide microstructure by TEM was also performed for the water-quenched and the air-cooled Zr–1.0 wt% Nb alloys showing the different corrosion resistance with cooling rate. Fig. 8 shows the oxide microstructure of air-cooled (Fig. 8(a)) and water-quenched (Fig. 8(b)) Zr–1.0 wt% Nb alloys having the same weight gain of about 20 mg/dm^2, respectively. The oxide microstructures were quite different from each other with the material condition even though the oxide thickness was almost the same. In the water-quenched specimen, the oxide morphology was an equiaxed structure and metal–oxide interface was wavy, while in the air-cooled specimen, the oxide morphology was columnar structure and metal-oxide interface was smooth. In case of considering this result in relation to oxide structure, it is thought that the corrosion resistance of the air-cooled specimen is better than that of the water-quenched specimen because the area fraction of grain boundary that is operated as a diffusion path of oxygen is higher in equiaxed structure (water-quenched specimen) than in columnar structure (air-cooled specimen).

3.4. Change of corrosion kinetics and microstructure during corrosion testing

Fig. 9 shows the corrosion behaviors of four kinds of Zr–xNb alloys with the different cooling rate corroded in steam at 400 °C for 150 days. As mentioned above, the difference of corrosion rate with cooling rate was appeared in the early stage of corrosion exposure until 60 days. Namely it was shown that the corrosion resistances of water-quenched and oil-quenched specimens of which cooling rates had been so fast, thereby supersaturating the added Nb in matrix, were remarkably bad in comparison with the corrosion resistance of air-cooled specimen. However, the gap of weight gain with cooling rate was getting narrow as corrosion exposure time increased from this point. In the specimens having Nb more than 1.0Nb, the corrosion rates of the specimens were gradually decreased after 60 days; however the air-cooled specimen showed still higher corrosion rate than water-quenched and oil-quenched specimen. Fig. 10 shows the change of the weight gain with cooling rate for the specimens corroded for 60 (a) and 150 days (b) respectively. The corrosion rates of high Nb alloys (1.0, 2.0, 3.0 wt% Nb) which had shown the significant difference of weight gain between the water-quenched and the air-cooled specimen before 60 days gradually decreased with exposure time after 60 days, and then reached to the weight gain of air-cooled specimens at 150 days.

Many studies on Zr–Nb binary alloy system have been carried out relating to the phase transformation by aging below monotectoid temperature (610 °C) [8–11]. In this work, the effect of cooling rate on the corrosion was observed in an early stage of corrosion. Namely, the corrosion resistance was deteriorated with increasing cooling rate. However, after corrosion testing for 150 days, the corrosion resistance was similar in all the specimens having the same Nb content regardless of the cooling rate. Consequently, the microstructural change during corrosion testing in steam at 400 °C was conjectured. Thus, in order to confirm whether a phase transformation during corrosion testing in high temperature and pressure occur or not, the microstructural observation for the water-quenched and the air-cooled Zr–xNb ($x = 1.0$, 3.0 wt%) alloys corroded in steam at 400 °C for 150 days was performed by using TEM. As shown in Fig. 11, in the case of the water-quenched

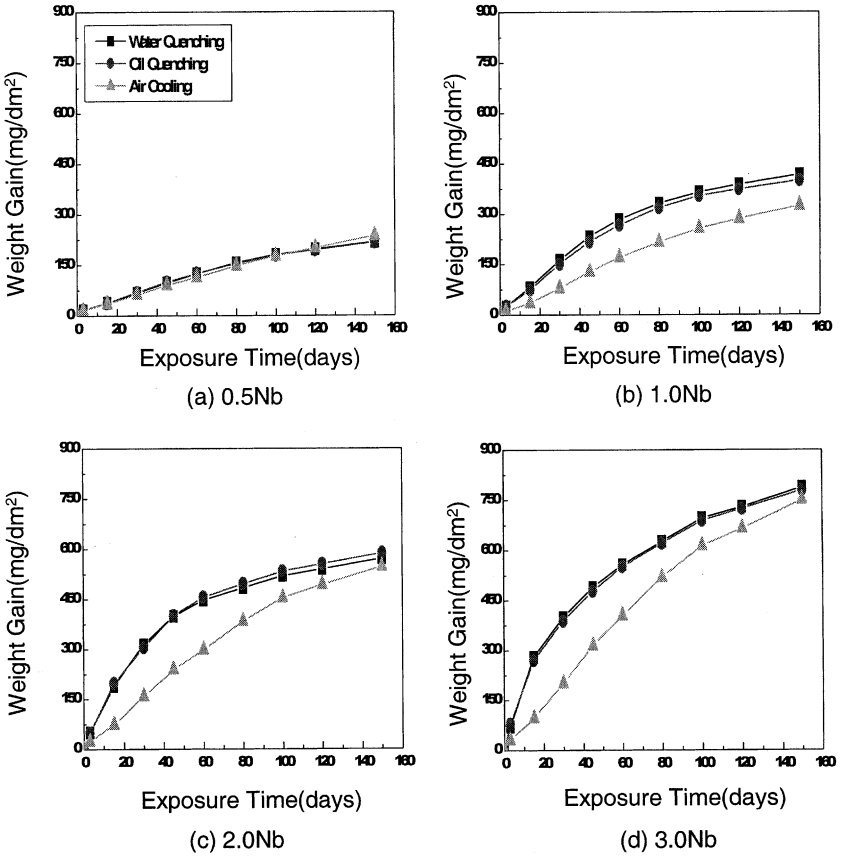

Fig. 9. The effect of cooling rate on the corrosion behavior of Zr–xNb alloys corroded at 400 °C steam for 150 days.

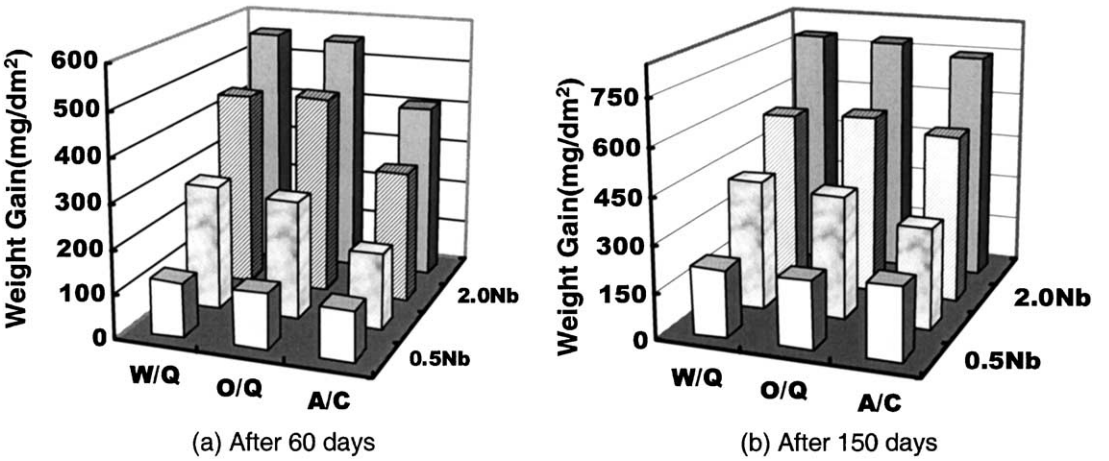

Fig. 10. Relationship between cooling rate, Nb content and corrosion weight gains in 400 °C steam for (a) 60 days and (b) 150 days. (W/Q: water quenching, O/Q: oil quenching A/C: air cooling.)

specimens having martensitic structure, the dislocation density was decreased considerably in comparison with that of the specimens before corrosion testing, and the fine particles were precipitated predominantly at twin and plate boundaries. From the result of EDS analysis the particles precipitated at twin boundary and plate

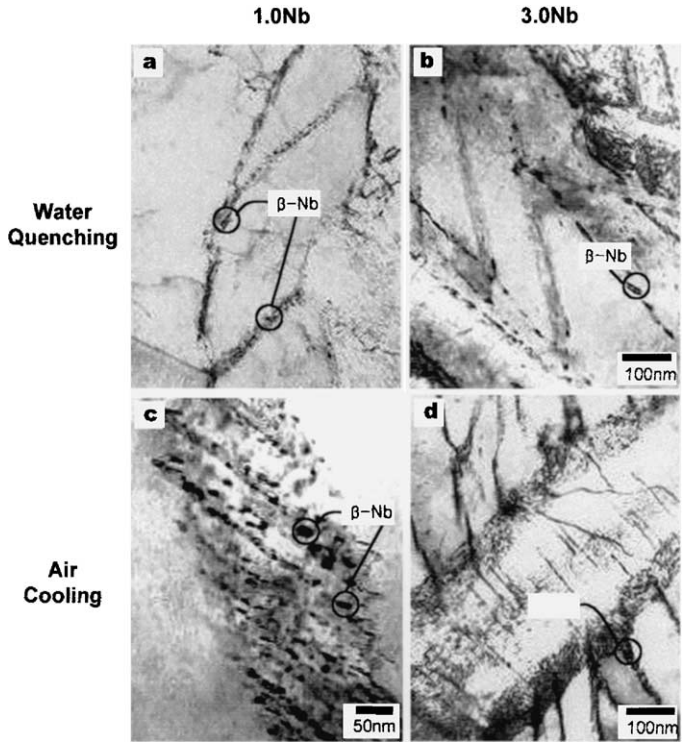

Fig. 11. TEM micrographs of Zr–xNb ($x = 1.0$, 3.0 wt% Nb) alloys corroded at 400 °C steam for 150 days.

boundary were identified as β_{Nb} phase. It was reported in the earlier works by Sabol [22] and Williams [23] that β_{Nb} phase could precipitate by aging the β-quenched Zr–2.5 wt% Nb alloy. From this result, it is considered that during corrosion testing the supersaturated Nb in matrix of the water-quenched and the oil-quenched specimens precipitates as a most part of β_{Nb} phase that contains about 80 wt% Nb. Thus, the Nb concentration in α matrix would be lowered up to solubility limit of Nb. As a result, it seemed that the soluble equilibrium Nb concentration in α matrix of water-quenched and oil-quenched specimen was similar to that of air-cooled specimen. And in the case of air-cooled specimens, Nb concentration in α matrix was similar to the value before corrosion testing. However it was observed that continuous film-like β_{Zr} phase before corrosion testing was decomposed to the fine particles. It was reported that β_{Zr} phase could be decomposed to the ($\alpha_{Zr} + \beta_{Nb}$) phases by annealing in the temperature range of 400–600 °C [10,11]. From this study, it was thought that such decomposition also would occur during long-term (150 days) corrosion testing at 400 °C and 1500 psi. In the early stage of corrosion testing, the amount of supersaturated Nb was higher in the water-quenched specimen than in the air-cooled specimen; consequently the weight gain of water-quenched specimen was higher than that of air-cooled specimen. But during corrosion testing for 150 days, the supersaturated Nb concentration of water-quenched specimen was decreased up to the equilibrium Nb concentration owing to the precipitation of β_{Nb}. Thus the corrosion resistance of water-quenched and oil-quenched specimen was increased gradually with exposure time in autoclave.

4. Conclusion

In the water-quenched and the oil-quenched specimens of which cooling rates were so fast, the martensitic structure was observed without formation of beta phase or precipitates, while in the air-cooled specimens, the coarse plate structure was observed with formation of β_{Zr} phase at plate boundary.

In the Zr–0.5 wt% Nb alloys that contain Nb less than solid solution limit (0.6 wt%) in Zr matrix, there was no difference of the corrosion resistance in spite of showing the different microstructures with cooling rate. This means that the corrosion resistance of Zr–0.5 wt% Nb alloy is not controlled by the microstructure such as dislocation, twin, and plate. In Zr–xNb alloys that contain Nb more than 0.6 wt%, the corrosion resistance of the specimens was deteriorated with increasing the supersaturated Nb concentration in matrix and the area fraction of β_{Zr} phase. It is suggested that the corrosion

resistance is enhanced when Nb exists in equilibrium state below solubility limit, while the corrosion resistance is decreased when Nb exists in supersaturated state above solubility limit or β_{Zr} phase.

During the corrosion testing at 400 °C, the microstructures of the specimens were gradually changed with exposure time. In the case of water-quenched and oil-quenched specimens having martensitic structure, the fine β_{Nb} phase was formed at plate and twin boundaries, and in the air-cooled specimens, the β_{Zr} phase was decomposed into ($\alpha_{Zr} + \beta_{Nb}$) phases. Therefore, the gap of weight gain with cooling rate in the early stage of corrosion test was getting narrow as the corrosion exposure time increased, and then after corrosion test for 150 days, the corrosion resistance was similar in all the specimens having the same Nb content regardless of the difference of microstructures.

It is summarized from the microstructural study and corrosion test with variation of cooling rate and Nb content that the equilibrium Nb concentration below solubility limit in α matrix plays more important role to enhance the corrosion resistance than the supersaturated Nb, the beta phase, and the precipitates.

Acknowledgements

This project has been carried out under the Nuclear Fuel R&D program by KAERI.

References

[1] G.P. Sabol, G.R. Kilp, M.G. Balfour, E. Roberts, Zirconium in the Nuclear Industry, ASTM Spec. Tech. Publ. 1023 (1989) 227.
[2] K. Yamate, A. Oe, M. Hayashi, T. Okamoto, H. Anada, S. Hagi, in: Proceedings of the 1997 International Topical Meeting on LWR Fuel Performance, Portland, OR, 2–6 March, 1997, p. 318.
[3] J.P. Mardon, G. Garner, P. Beslu, D. Charquer, J. Senevat, in: Proceedings of the 1997 International Topical Meeting on LWR Fuel Performance, Portland, OR, 2–6 March, 1997, p. 405.
[4] V.F. Urbanic, R.W. Gilbert, in: IAEA Technical Committee Meeting on Fundamental Aspects of Corrosion of Zr-based Alloys for Water Reactor Environments, Portland, OR, 11–15 September, 1989, p. 262.
[5] V.F. Urbanic, M. Griffith, Zirconium in the Nuclear Industry, ASTM Spec. Tech. Publ. 1354 (2000) 641.
[6] H.G. Kim, Y.S. Lim, M.Y. Wey, Y.H. Jeong, J. Kor. Inst. Met. Mater. 37 (1999) 584.
[7] Y.H. Jeong, Kor. J. Mater. Res. 6 (1996) 585.
[8] G.P. Sabol, R.J. Comstock, U.P. Nayak, Zirconium in the Nuclear Industry, ASTM Spec. Tech. Publ. 1354 (2000) 525.
[9] S. Banerjee, S.J. Vijayakar, R. Krishnan, J. Nucl. Mater. 62 (1976) 229.
[10] S.A. Aldridge, B.A. Chedle, J. Nucl. Mater. 42 (1972) 32.
[11] M.T. Javanovic, Y. Ma, R.L. Eadie, J. Nucl. Mater. 244 (1997) 141.
[12] Nishiyama, Martensitic Transformation, Academic Press, New York, 1978, p. 6.
[13] C.E.L. Hunt, P. Niessen, J. Nucl. Mater. 38 (1971) 17.
[14] D.A. Porter, K.E. Easterling, Phase Transformation in Materials, Chapman and Hall, London, 1992, p. 410.
[15] K.N. Choo, Y.H. Kang, S.I. Pyun, V.F. Urbanic, J. Nucl. Mater. 209 (1994) 226.
[16] E. Hillner, A.L. Low, G.W. Perry (Eds.), Zirconium in the Nuclear Industry, ASTM Spec. Tech. Publ. 633 (1977) 211.
[17] V.F. Urbanic, B.D. Warr, A. Manolescu, C.K. Chow, M.W. Shanahan, Zirconium in the Nuclear Industry, ASTM Spec. Tech. Publ. 1023 (1988) 20.
[18] J. Godlewski, Zirconium in the Nuclear Industry, ASTM Spec. Tech. Publ. 1245 (1994) 663.
[19] H.J. Beie, A. Mitwalsky, F. Garzarolli, H. Ruhmann, H.J. Sell, Zirconium in the Nuclear Industry, ASTM Spec. Tech. Publ. 1245 (1994) 615.
[20] H. Anada, K. Takeda, Zirconium in the Nuclear Industry, ASTM Spec. Tech. Publ. 1295 (1996) 35.
[21] H. Anada, B.J. Herb, K. Nomoto, S. Hagi, R.A. Graham, T. Kuroda, Zirconium in the Nuclear Industry, ASTM Spec. Tech. Publ. 1295 (1996) 74.
[22] G.P. Sabol, J. Nucl. Mater. 34 (1970) 142.
[23] C.D. Williams, R.W. Gilbert, J. Nucl. Mater. 18 (1966) 161.